EFDA–JET–CP(14)01/11

H. Bergsåker, I. Bykov, P. Petersson, G. Possnert, J. Likonen,
S. Koivuranta, J.P. Coad, W. Van Renterghem, I. Uytdenhouwen,
A.M. Widdowson and JET EFDA contributors

Microscopically Nonuniform Deposition and Deuterium Retention in the Divertor in JET with ITER-like wall

Microscopically Nonuniform Deposition and Deuterium Retention in the Divertor in JET with ITER-like wall

H. Bergsåker[1], I. Bykov[1], P. Petersson[1], G. Possnert[2], J. Likonen[3], S. Koivuranta[3], J.P. Coad[3], W. Van Renterghem[4], I. Uytdenhouwen[4], A.M. Widdowson and JET EFDA contributors*

JET-EFDA, Culham Science Centre, OX14 3DB, Abingdon, UK

[1]Department for Fusion Plasma Physics, Association EURATOM-VR, School of Electrical Engineering, Royal Institute of Technology, S-10405 Stockholm, Sweden
[2]Uppsala Universitet, Tandem Laboratory, Association EURATOM-VR, S-75105 Uppsala, Sweden
[3]VTT, Association Euratom-Tekes, PO Box 1000, FI-02044 VTT, Finland
[4]SCK·CEN, Institute for Nuclear Material Sciences, Boeretang 200, 2400 Mol, Belgium
** See annex of F. Romanelli et al, "Overview of JET Results", (24th IAEA Fusion Energy Conference, San Diego, USA (2012)).*

Preprint of Paper to be submitted for publication in Proceedings of the 21st International Conference on Plasma Surface Interactions, Kanazawa, Japan 26th May 2014 – 30th May 2014

ABSTRACT

The divertor surfaces in JET with ITER-like wall (ILW) have been studied using micro ion beam analysis (μ-IBA) methods and scanning electron microscopy (SEM). Deposited layers with beryllium as main constituent had been formed during plasma operations through 2011–2012. The deuterium trapping and impurity deposition were non-uniform, frequently enhanced within regions reaching in size from 10μm to 200μm. Enhanced amounts of D and impurities were found at pits, cracks and valleys in the tungsten coating. The impurity deposition and fuel retention were correlated with the surface slope with respect to the direction of ion incidence. Typically more than 70% of the total measured areal density of trapped D was found in less than 30% of the surface area. This of consequence for the interpretation of other surface analyses and in extrapolation from fuel retention in JET with ITER-like wall and rough divertor surfaces to ITER with smoother surfaces.

1. INTRODUCTION

The migration of materials in large fusion devices is of concern particularly in view of the trapping of fuel at surfaces through co-deposition with wall material [1]. Where more than one plasma facing material is used, the mixing of materials due to migration is likewise an issue. It has been shown that the net deposition rate of a ^{13}C marker impurity at a limiter surface can be enhanced by a factor 3-5 by surface roughness [2]. Early microanalysis of plasma exposed surfaces from AUG and TEXTOR showed that impurities (B and C) were net deposited preferentially in depressed surface regions, such as pre-existing or plasma produced pits, cracks and arc tracks [3]. Preferential net deposition of metal impurities was also observed in pits at CFC surfaces of limiters in TEXTOR [4] and microscopic investigation of W coated CFC surfaces at JET with carbon wall (JET-C) showed microscopically non uniform erosion of W as well as preferential net C deposition in depressed surface areas [5]. Microscopically nonuniform fuel trapping has received growing attention in recent years, in particular post mortem microanalysis of surfaces after plasma exposure in JET-C [6-12], Tore Supra [13-16], TEXTOR [17], PISCES-A [17] and AUG[18]. Ion beam analysis with micro beam has been a particularly useful tool for elemental mapping, either of deposited layer cross sections [6, 8,9,11] or of the surface [7, 9, 10, 12-17]. Typically the spatial resolution with this method has been 5-15μm. It has been possible by careful selection of the area of interest on the surfaces, or by elemental mapping with EDX, to compare directly the elemental distribution with microscopic images of layer structures and surface/interface topography, correlating regions of enhanced accumulation of impurities and deuterium with topographic features with sizes in the range 10-200μm [4,5,9,10,12-14,18]. A related problem, which has been investigated is that of impurity deposition and fuel trapping inside castellation gaps with widths of about 500μm [19].

Attempts to model the erosion and deposition at rough surfaces include numerical simulation of particle incidence at a realistic rough surface following the acceleration through flat magnetic pre-sheath and electrostatic sheath [20] and detailed treatment of different species derived from an ERO simulation impacting a schematic rough surface [21]. The deposition inside castellation gaps

has been modelled with ERO-3D-GAPS [19], with a possibility to include particle in cell (PIC) simulations of plasma penetration into narrow gaps [22].

It is essential to investigate the microscopic distribution of impurity deposition and fuel retention and its relation to surface roughness from the points of view of understanding where and how fuel is trapped, to interpret surface analysis results correctly and to make reliable extrapolations, e.g. from JET with ITER-like wall (JET-ILW) to ITER (with initially smooth, although castellated) W surfaces in the divertor. It is also relevant to the assessment of methods for removal of fuel trapped at surfaces. This report shows how deuterium and impurities are distributed microscopically at the surfaces of the JET divertor following the first operations with ITER-like wall and the relation to surface topography.

2. EXPERIMENTAL

Figure 1 shows a poloidal cross section of the JET divertor. With the exception of Tile 5, the divertor tiles are W coated CFC. Also shown are three representative plasma shapes. As in the carbon wall phase [8-12], samples were taken from selected tiles following operations in 2011–2012 using a coring method. The sample surfaces were scanned with ion microbeam at the tandem laboratory at Uppsala University [6, 10, 12]. Nuclear reaction analysis (NRA) with 3MeV $^{3}He^{++}$ beam was used for mapping of D, Be and C. Copper grids were attached on the sample surfaces for accurate identification of the areas of interest. Mapping of Cu, Cr, Fe, Ni, Mo and W was made by characteristic X-rays (PIXE). The X-ray yield from the Cu grids was used also for current integration. Nuclear reaction products were measured with an annular detector at about 15° from the surface normal, covering all azimuthal angles, with little shadowing due to surface roughness. X-rays were detected at 45° from normal, leaving room for some shadowing effects. The quantification methods are described in [6, 12] and the averaging and presentation methods and image processing are described in detail in [12]. While for thick targets calibrations using elemental targets were used [6], thin and intermediate layer analysis relies on literature cross sections [23,24]. The areas of interest were imaged also with scanning electron microscopy (SEM) and the images were overlaid so that the elemental distributions can be compared directly with surface topography. Stereo SEM was used to determine the topography, as shown in [12]. Polished cross sections as well as raw cross section cuts of the W layers and the layers deposited through JET plasma operation were also studied with optical microscopy and SEM.

3. RESULTS

Figure 2 shows proton spectra from the $D(^{3}He,p)^{4}He$ reaction, starting from about 11.3MeV, integrated over about 250μm x 200μm regions at different positions in the divertor. The spectra carry depth information, with the low energy edge corresponding to the surface and higher energies to larger depths. The rear (blue) spectrum is from position 4/10 in JET-C. The layer was much thicker than the range of 3MeV ^{3}He ions and the D concentration was nearly uniform, so the reason for the

high energy drop in the spectrum at about 12.9MeV is the drop in the nuclear reaction cross section below 0.6MeV ^{3}He [23] and determines the matrix dependent accessible depth for the D analysis. For Be matrix with density 1.8g/cm^3 the accessible depth is about 12μm, for C matrix with density 1g/cm^3 it is 18μm and for W matrix with 19g/cm^3 it is 4μm. In principle, when the beam is scanned and the beam position is read and stored in coincidence with every detected proton, 3D information about the deuterium distribution can be obtained. However, the due to poor statistics the data do not allow a full 3D reconstruction and as in [10, 12] the spectra are coarsely divided into a shallow contribution and a deep contribution. The spectra in Figure 2 from Tiles 1, 4 and 7 all suggest thin surface layers with high D concentration, but all except 4/10 with ITER-like wall also show deeply situated D, down to the accessible depth. The spectrum shown for position 7/7, with a well separated deeply buried D rich region is typical for the spectra from the outer divertor. Also shown in Figure 2 at about 9.8MeV and extending downwards, is the p_0 peak from the ^{9}Be(^{3}He,p)^{11}B reaction, used for Be analysis. In this case the surface corresponds to the highest energy. It is important to realize that each spectrum in Figure 2 is the result of a superposition of spectra from microscopic regions with very different compositions.

Figure 3 shows maps of Be, shallow D and deep D in a surface region at position 1/10. The images are oriented so that the toroidal magnetic field and the parallel ion drift towards the surface are both from right to left. High areal density of Be is found associated with the vertical crack on the lower right hand side of the scanned area, as well as with the two horizontal cracks propagating on the left hand side of the central hole. Large amounts of Be are also found in the wide area above the hole, which includes a crack and a flat area to the left of it. Not much Be is found in the hole or at the rims of the hole, except on the left hand side of the hole. With grazing magnetic field the plasma can penetrate slightly further into the hole on the left hand side, so the edge there will be called plasma wetted [19,22].

Deuterium is also found at some of the cracks, but predominately around the edges of the hole. Other pits at 1/10 shows Be at the plasma wetted sides of pits, deep D around the edges inside pits and shallow D at the plasma shadowed edges. At 1/8 the Be distribution was uniform, while deep D was found predominantly on the plasma wetted side of vertical ridges at the surface, and shallow D in valleys between ridges. Elemental maps of Be, C, N and D at position 3/6 are shown in [12]. They are all accumulated at pits, cracks and depressed regions, especially at the edges of larger pits, the impurities with preference for the plasma wetted edges. At position 4/10 the maps of Be, C and D are uniform, in particular with no enhancement in pits. At 4/6, again Be and D are found mainly at pits and cracks, especially on the plasma wetted side of a large pit. Figure 4 shows maps of Be, D and Inconel components associated with a large hole in the substrate at position 6/7. A surface height map from stereo SEM is shown in Figure 3b. In this case the toroidal field direction is from right to left, but the ion parallel flow towards the surface is from left to right. Both impurities and D in this case seem to have accumulated on the plasma shadowed side of the hole. So far we have only discussed the right/left asymmetry. In these maps there is also an up/down

asymmetry in that D and impurities appear to be accumulating preferably on the upper side edges of the pit. In this figure as well as in Figure 3, the gyration direction of the ions approaching the surface is preferentially upwards (direction of ion diamagnetic drift). Also the D accumulation in a large pit at position 3/6 is predominantly at the edge where highest ion flux is expected due to the gyration [12], c.f. [22]. Another likely effect of ion angle of incidence is the alignment of elongated structures shown in Figure 5. There are aligned structures elongated of different types, notably the conical structures found in the area on Tile 3 with frequent strike points (Figure 5 c), reminiscent of some of the structures in Be that have been observed on samples exposed in PISCES-B [25]. On the vertical parts of Tiles 1 and 3, elongated structures like these are consistently oriented from upper left to lower right, i.e. toroidally towards negative toroidal angle and slightly downwards, while on Tile 6 they are oriented towards positive toroidal angle and slightly radially outwards, hence consistently towards the direction from which ions would tend to arrive, including parallel drift and gyro motion.

4. DISCUSSION

Except for the upper horizontal surface of Tile 1, the deposition rate at the divertor surfaces was lower during ILW operation, compared to carbon wall [26]. Gas balance measurements have also shown that as expected [1] the long term deuterium retention with ILW was 10-20 times lower with ILW than with carbon wall [27]. The roughness of the CFC surfaces has carried over to the surface of the W coatings, resulting in a roughness of ~10μm [28]. As in JET-C [9, 10, 12] and in many other devices, enhanced net deposition and deuterium retention is associated with pits, cracks and depressed regions at the surface. This was seen at all the studied divertor surfaces from JET-ILW, except at position 4/10, where deposition is believed to be due to neutral species. In JET-C, regions with preferential trapping of deuterium were found not only at layer the surface, but also at pits in the original CFC surface. In that case, not only was there an accumulation of deposited material inside pits in the CFC, but the deuterium concentration could also be higher inside such pits, compared to the bulk of the deposited layers that (Figure 3 of ref. [10]). Buried regions with enhanced deuterium concentration could also be identified within the thick deposited layers. The deposited layers after the first period of operations with ITER-like wall were still too thin to distinguish features of this type. It has often been stated that deposited materials accumulate in microscopically shadowed regions. Still, the physical nature of this shadowing effect needs to be better understood. In most cases either overall erosion dominates [3,15-18,20,21], or there is a combination of erosion and deposition, with resulting overall net deposition [3,6-12,21]. Then, if shadowed microscopic regions are partly protected from erosion, the balance between erosion and deposition may be locally shifted there towards faster net deposition. Due to the grazing incidence of the magnetic field, the interior of pits in the surface are protected from the parallel heat flux carried by electrons. However, considering a heat diffusivity of the order $10^{-4}m^{-2}s^{-1}$ for W, pits of ~50μm dimension may be considered as thermally protected only to transient heat loads, of shorter duration

than about 25μs, while the heat diffusion length over a full JET plasma flat top is several cm. Pits are partly protected also from ion flux. A plausible conjecture then might be that pits are filled up by the flux of neutral species, just like thick layers with high deuterium concentration were growing in the divertor corner, far out on Tile 4 in JET-C [10]. However, there is frequently preferential deposition at the sides of pits where the slope is such that higher ion flux can be expected. Also different species are sometimes accumulated on different slopes. That the ion angle of incidence is significant for the deposition patterns is demonstrated also by the systematic direction of elongated structures, as shown in Figure 5. Columns in consistent directions have been observed in deposited carbon layers in tokamaks. At the outer dome wing in JT-60 [29] and at Tile 4/10 at JET-C [10] columns were tilted practically only in the poloidal direction and were explained by deposition of neutral species. At the vertical surfaces of the inner divertor in JET-C on the other hand, columns were directed typically as in Figure 5 [10], qualitatively in the direction of ion incidence, including gyro motion. In AUG as well, elongated structures have been observed aligned in approximately the same direction (at 40° with respect to the magnetic field) and enhanced deposition has been found on the side of protruding objects which would be in the shadow from the incident ion flux [18]. All this suggests that proper understanding of the deposition in pits requires detailed modelling of the ion trajectories [20,21]. One important factor then must be the size of the surface structures with respect to the Debye length (~ 10μm in the JET divertor) and ion Larmor radii (~ 100μm). The surface structures with observed preferential fuel and impurity accumulation ranges from about 1μm (like the cracks in Figure 3) to ~ 100μm (for large pits like in Figure 4).

Many of the surface features observed with SEM are of sizes that can be resolved with μ-IBA. This means that effects of locally slanted surface and variable matrix composition, which can be misleading in broad beam IBA, can be better interpreted. With thick deposits it is also important not to rely on the surface composition within the accessible depth for IBA for evaluating the composition of the whole layer. Studies of layer cross sections with μ-IBA have shown microscopically variable composition [8,9].

As evident from Figure 2, the analysis in this report does not access deep enough to measure the total retained areal density of deuterium. If deuterium and other species are mobile at the surfaces inside pits, cracks and channels, e.g. from the surface into the bulk of CFC, it may permit deuterium to penetrate, as suggested in [13, 15, 30].

A significant fraction of the deuterium retention at the divertor surfaces in JET-ILW is associated with trapping in pits and cracks. Typically more than 70% of the total measured areal density of trapped D is found in less than 30% of the surface area. For extrapolation to longer plasma exposure times it is important how the surface roughness develops. Both roughening [3,18,25] and smoothening [4] by plasma exposure has been reported.

Preferential deposition in pits obviously makes the surface smoother and the enhanced D retention in pits may cease, once the pits have been filled, as suggested by Figure 3 of ref. [10]. However, if new surface roughness is also created, the process may go on cumulatively, and in the thick deposited

layers in JET-C microscopic regions with enhanced D retention were found also at the surfaces of the layers and buried inside them [10]. The W coated CFC surfaces in JET-ILW are rougher than those of the ITER tungsten surfaces will be, at least initially. Thus one would expect that the fraction of D trapped in surface roughness in JET would either not be trapped at all in ITER, or would be migrating elsewhere. It is expected however that the divertor surfaces in ITER will develop cracks and surface roughness with time, due to transient heating [31] and possibly other effects, like H blistering [18], He holes, W-fuzz production and arcing [31].

5. CONCLUSIONS

Microscopically non uniform impurity deposition and deuterium retention has been found at the divertor surfaces in JET-ILW. In particular, impurities and deuterium have accumulated preferentially in pits, cracks and depressed regions on the surfaces exposed to ion flux. Typically more than 70% of the total measured areal density of trapped D at representative surfaces is found in less than 30% of the surface area. The asymmetric deposition at the edge sides of larger pits, as well as the consistent orientation of elongated surface structures shows that the predominant direction of ion incidence plays an important role for the layer growth.

ACKNOWLEDGEMENTS

This work was supported by EURATOM and carried out within the framework of the European Fusion Development Agreement. The views and opinions expressed herein do not necessarily reflect those of the European Commission.

REFERENCES

[1]. J. Roth, E. Tsitrone, A. Loarte et al. Journal of Nuclear Materials **390–391** (2009)1–9.
[2]. A. Kreter, S. Brezinsek, T. Hirai et al. Plasma Physics and Controlled Fusion **50** (2008)095008.
[3]. D. Hildebrandt, H. Grote, W. Schneider et al. Physica Scripta **T81** (1999)25–30.
[4]. M. Rubel, E. Fortuna, A. Kreter et al. Fusion Engineering and Design **81** (2006)211–219.
[5]. M. Mayer, J. Likonen, J.P. Coad et al. Journal of Nuclear Materials **363–365** (2007)101–106.
[6]. H. Bergsåker, B. Emmoth, P. Petersson et al. Journal of Nuclear Materials **362** (2007)215–221.
[7]. L.C. Alves, E. Alves, N.P. Barradas et al. Nuclear Instruments and Methods **B268** (2010)1991.
[8]. P. Petersson, H. Bergsåker, G. Possnert et al. Journal of Nuclear Materials **415** (2011) S262-S265.
[9]. H. Bergsåker, P. Petersson, I. Bykov et al. Journal of Nuclear Materials **438** (2013)S668-S672.
[10]. H. Bergsåker, I. Bykov, P. Petersson et al. Nuclear Instruments and Methods B in press, http://dx.doi.org/10.1016/j.nimb.2014.02.075
[11]. I.Bykov, H.Bergsåker, P. Petersson et al. Nuclear Instruments and Methods B. in press, http://dx.doi.org/10.1016/j.nimb.2014.02.078
[12]. "Combined ion micro probe and SEM analysis of strongly non uniform deposits in fusion devices", I. Bykov, H. Bergsåker, P. Petersson et al. Nuclear Instruments and Methods B submitted.

[13]. H. Khodja, C. Brosset and N. Bernier, Nuclear Instruments and Methods **B266** (2008)1425 –1429.
[14]. P. Pelicon, P. Vavpetic, N Grlj et al. Nuclear Instruments and Methods **B269** (2011)2317.
[15]. P. Petersson, G. Possnert, M. Rubel et al. Journal of Nuclear Materials **415** (2011)S761–S764.
[16]. P. Petersson, H. Bergsåker, G. Possnert et al. Journal of Nuclear Materials **415** (2011)S262–S265.
[17]. P. Petersson, A. Kreter, G. Possnert et al. Nuclear Instruments and Methods **B268** (2010)1833.
[18]. M. Balden, V. Rohde, S. Lindig et al. Journal of Nuclear Materials **438** (2013)S220–S223.
[19]. D. Matveev, A. Kirschner, A. Litnovsky et al. Plasma Physics and Controlled Fusion **52** (2010) 075007
[20]. K. Schmid, M. Mayer, C. Adelhelm et al. Nuclear Fusion **50** (2010)105004.
[21]. S. Dai, A.Kirschner, D.Matveev et al. Plasma Physics and Controlled Fusion **55** (2013)055004.
[22]. M. Komm, R. Dejarnac, J.P. Gunn et al. Plasma Physics and Controlled Fusion **55** (2013)025006.
[23]. V. K. Alimov, M. Mayer, J. Roth et al. Nuclear Instruments and Methods **B234** (2005)169.
[24]. E. A. Wolicki et al. Physical Review. **116** (1959)1585.
[25]. R.P. Doerner, M.J. Baldwin and D. Nishijima, Journal of Nuclear Materials **455** (2014)1–4.
[26]. A. Widdowson, E. Alves, C.F. Ayres et al. Physica Scripta **T159** (2014)014001.
[27]. S. Brezinsek, T. Loarer, V. Philipps et al. Nuclear Fusion **53** (2013)083023.
[28]. J. Likonen, E. Alöves, A. Baron-Wiechec et al. Physica Scripta **T159** (2014)014016.
[29]. Y. Gotoh, T. Tanabe, Y. Ishimoto et al. Journal of Nuclear Materials **357** (2006)138–146.
[30]. M. Rubel, B. Emmoth, H. Bergsåker et al. Journal of Nuclear Materials **196–198** (1992)285–291.
[31] Y. Ueda, J.W. Coenen, G. De Temmerman et al. Research status and issues of tungsten plasma facing materials for ITER and beyond, Fusion Engineering and Design (2014), http://dx.doi.org/10.1016/j.fusengdes.2014.02.78.

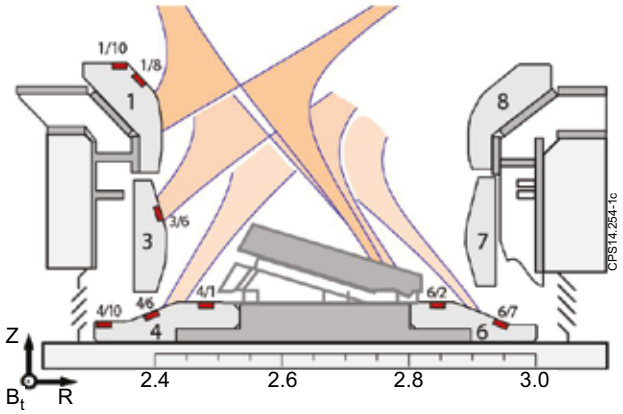

Figure 1: Poloidal cross section of the JET divertor, showing the tile numbering and the positions of surface samples that are discussed. Also shown are three representative plasma shapes.

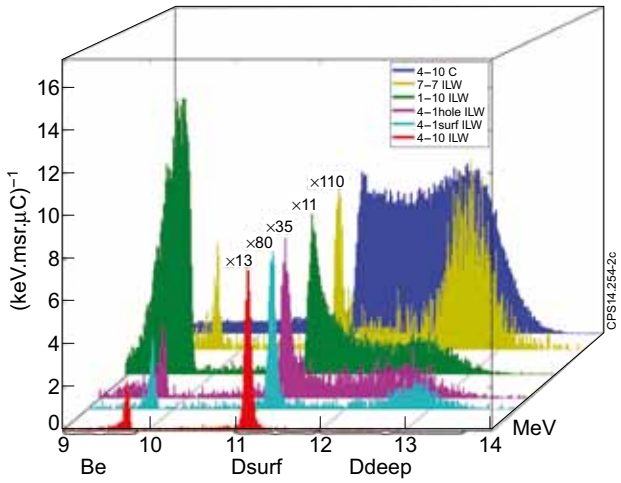

Figure 2: Examples of proton spectra, integrated over selected surface areas. The spectrum between 11MeV and 13MeV is related to the depth distribution of deuterium, while the peak extending downwards from 9.8MeV is from beryllium. All shown D spectra except that from position 4/10 with ITER-like wall extend to the accessible depth for the analysis (about 12μm in case of Be matrix). The energy intervals corresponding to shallow and deep deuterium are defined.

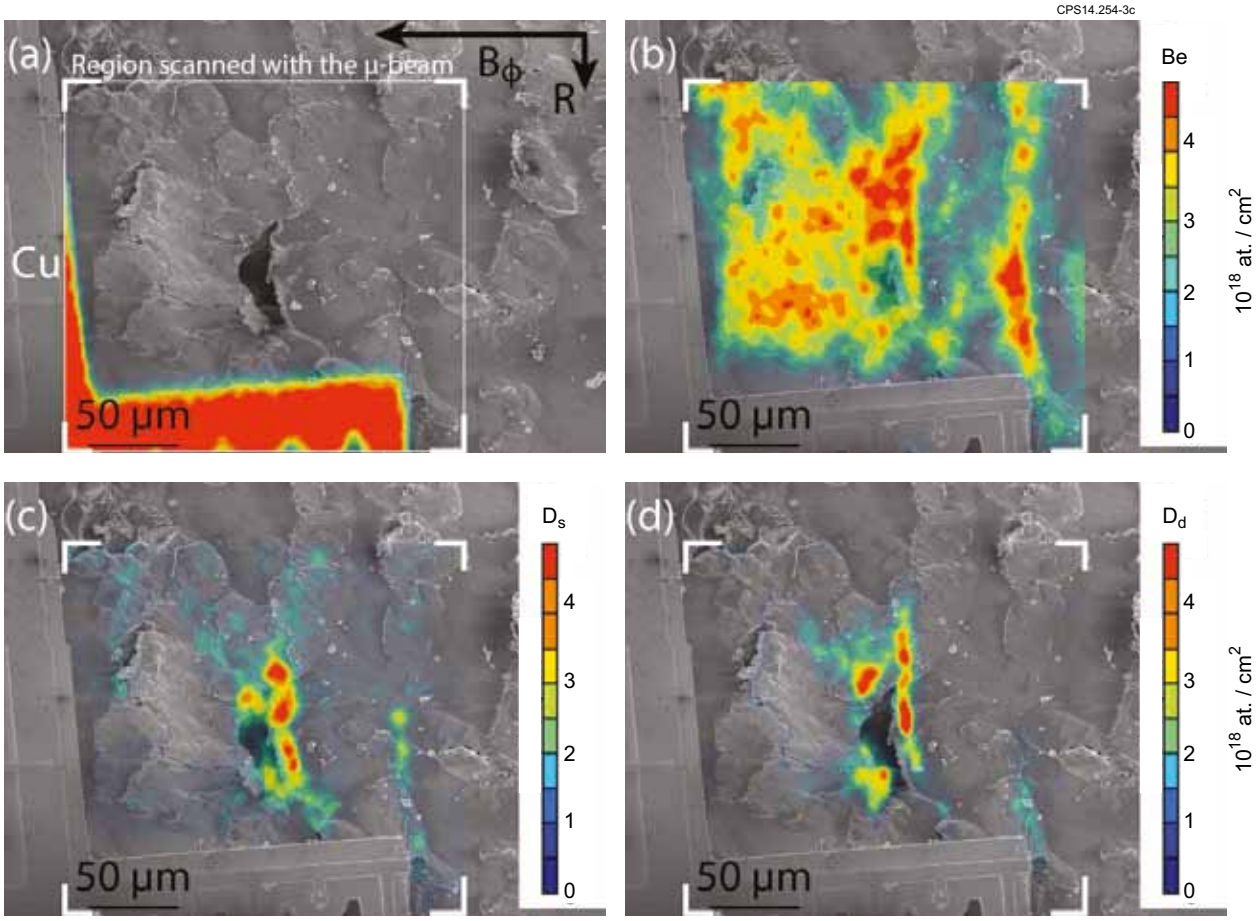

Figure 3: Elemental maps of a region at position 1/10. a) Cu grid used for positioning and current integration. b) Beryllium ma, with enhanced Be deposition at cracks and in the large area above the pit at the centre. c) Surface D, found mainly at cracks and at the shadowed side edge of the pit d) Deep deuterium, at cracks and around the edges of the pit.

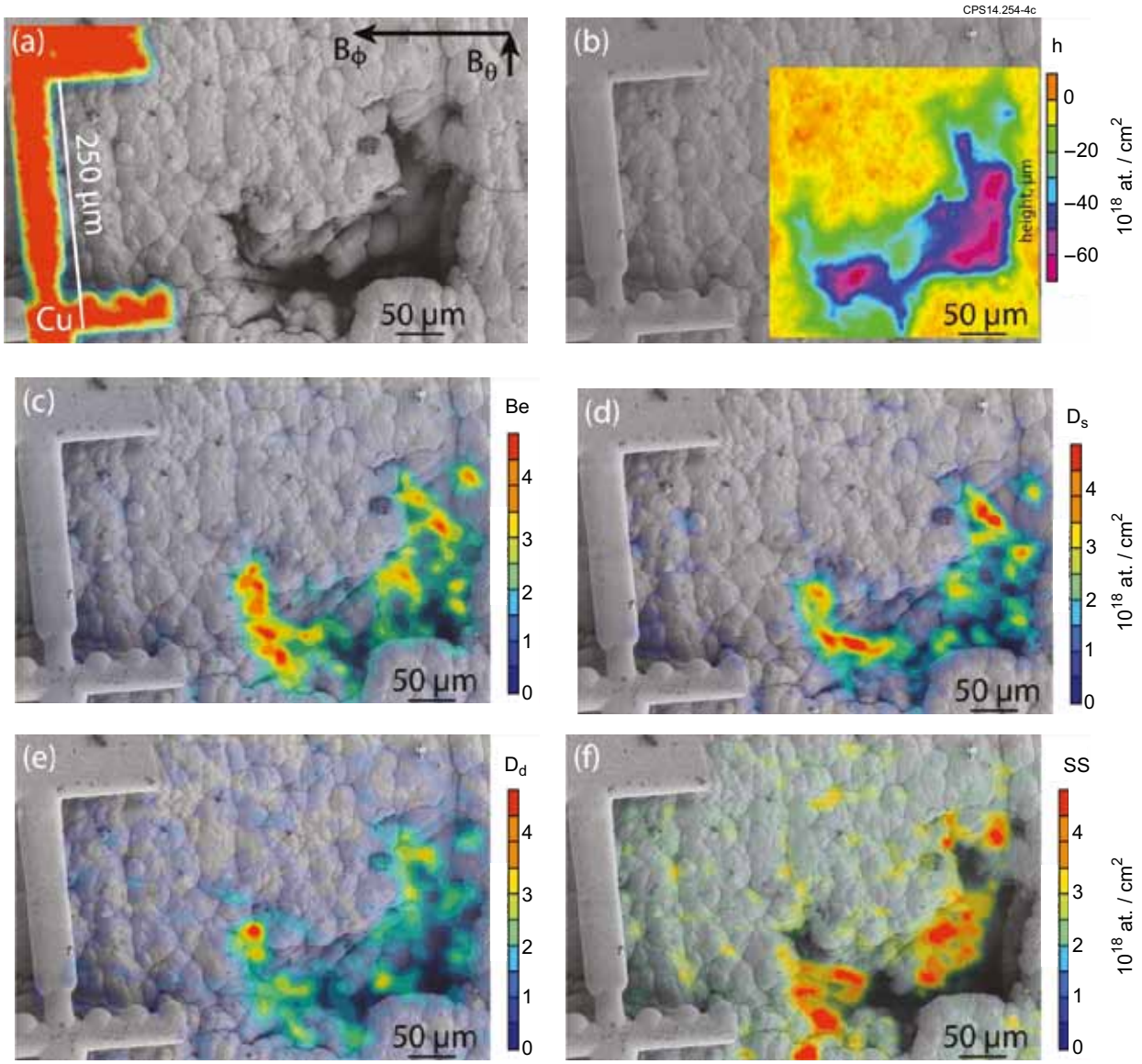

Figure 4. Elemental maps around a pit in the W coating at position 6/7. a) Cu grid used for positioning and current integration. b) Surface height map derived from stereo SEM. c) Be is found mainly on the upstream (plasma shadowed) side of the pit and on the upper side. d) Surface deuterium. e) Deep deuterium. f) Combined map of Cr, Fe, Ni .

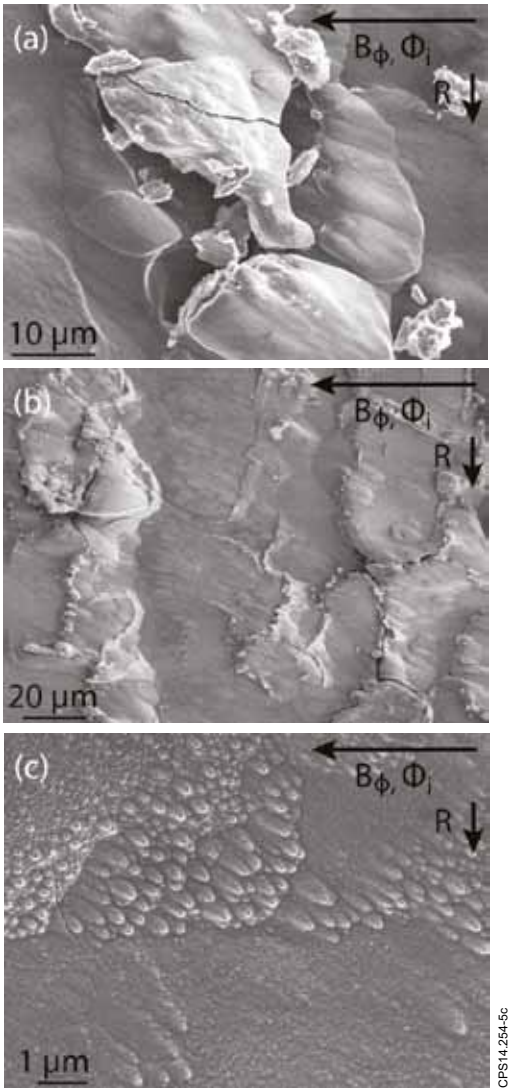

Figure 5. SEM images of the surfaces at 1/10 (a) 1/8 (b) and 3/6 (c). All surfaces show elongated structures that are pointing in a direction 15–20° downwards, with respect to the toroidal direction. The region (c) is slightly depressed with respect to the surrounding layer and has about 4µm Be deposited, so it seems likely that the cone like structure consists mainly of Be.